RSC Advances

PAPER

View Article Online
View Journal | View Issue

Cite this: *RSC Adv.*, 2023, **13**, 3890

An electrochemical aptasensor based on AuNRs/AuNWs for sensitive detection of apolipoprotein A-1 (ApoA1) from human serum

Raudhatul Husna,[a] Chitra Padmakumari Kurup,[b] Mohd Afaque Ansari,[a] Noor Faizah Mohd-Naim[ab] and Minhaz Uddin Ahmed *[a]

For early detection and diagnosis of cancer, it is essential to develop an electrochemical biosensor that is quick, accurate, and sensitive. Here, we use gold nanorod (AuNR) and gold nanowire (AuNW) nanocomposites (AuNR/AuNW/CS) as electrode modifiers on a glassy carbon electrode (GCE) to construct a sensitive label-free electrochemical aptasensor to detect ApoA1. The thiolated ApoA1-specific aptamers were immobilized onto the modified electrode surface through self-assembled monolayers. Electrochemical techniques, such as cyclic voltammetry (CV) and differential pulse voltammetry (DPV), were used to analyze the fabrication steps. The concentration of ApoA1 was measured with DPV on the aptasensor, with a linear range of 0.1 to 1000 pg mL^{-1} and a detection limit of 0.04 pg mL^{-1}. When compared to results from ELISA tests (which have a detection limit of 80 pg mL^{-1}), the results achieved here were over 2000 times better. The aptasensor's performance was successfully evaluated using human serum spiked with ApoA1, suggesting that it has great potential for practical application. The electrochemical apatsensor additionally demonstrated outstanding selectivity responses and strong stability toward the target analyte.

Received 19th October 2022
Accepted 23rd January 2023

DOI: 10.1039/d2ra06600a

rsc.li/rsc-advances

Introduction

In the field of advancement of biosensors for the early detection of diseases, electrochemical biosensors have been proven to be one of the promising techniques because of their robustness, higher sensitivity, and selectivity.[1] However, sample preparation, detection time, and real-time sensing are a few of the foremost obstacles associated with the early detection of diseases that need to be addressed.[2]

The signal amplification strategy is expected to increase a biosensor's detection sensitivity.[1] Consequently, numerous methods for signal amplification have been investigated, some of which focused on the amplification of nucleic acids, or the specific material being incorporated. Some examples of nucleic acid amplification strategies are rolling circle amplification, hybridization chain reaction, and enzyme-catalyzed signal amplification.[2] Nanomaterial-based signal amplification has been successfully employed in constructing a biosensor because of the tunable small size, large specific surface area, improved conductivity, and enhanced molecule adsorption of nanomaterials.[3,4] By enabling direct electron transfer between biomolecules and electrode surfaces, metals are excellent signal amplifiers in electrochemical biosensors.[2] Among various noble metals, gold nanomaterials are extensively used in biosensor applications due to their biocompatibility, optical and electronic properties, and relatively simple production and modification.[5–7] In addition to surface atom coverage, changes in form can also influence electro-catalytic activity, which may lead to an increase in activity.[3] Gold nanomaterials with different nanostructures, including spheres, rings, rods, and cages, were implicated in the modification of electrochemical sensors.[8–12] Non-spherical gold nanoparticles, such as gold nanorods (AuNR), have received considerable attention due to their unique optical properties, faster electron transfer ability, higher surface area, and strong light-scattering properties.[8] Moreover, AuNRs have shown greater load capacity and superior electrical conductivity.[13] Another non-spherical gold nanoparticle of interest is gold nanowires (AuNWs), which possess good conductivity, electron transport, and increased analytical sensitivity. Additionally, it features many exposed surface atoms, a distinctive quantum size effect, outstanding biocompatibility, and high flexibility.[14,15] A multifunctional nano-platform can be created by combining AuNRs and AuNWs with various other materials. For instance, a reduced graphene oxide (ERGO) and gold nanowires (AuNWs)-based electrochemical biosensor that accurately detected serum miR-137 was developed by Azimzadeh's group.[15]

Furthermore, the inclusion of chitosan (CS), a versatile, biocompatible, and non-toxic biopolymer in biosensor construction, has been reported.[16] CS is produced by deacetylating the

[a]*Biosensors and Nanobiotechnology Laboratory, Integrated Science Building, Faculty of Science, Universiti Brunei Darussalam, Jalan Tungku Link, Gadong BE 1410, Brunei Darussalam. E-mail: minhaz.ahmed@ubd.edu.bn; minhaz.ahmed@outlook.com*

[b]*PAPRSB Institute of Health Sciences, Universiti Brunei Darussalam, Jalan Tungku Link, Gadong BE 1410, Brunei Darussalam*

protein chitin, naturally found in shellfish.[11] It can attach nanoparticles to the working electrode's surface and help immobilize bioreceptors. Substrate materials should be non-toxic and contain functional groups; chitosan meets all of these criteria. The mechanical stability, immobilization, and reusability of the biological response elements and nanostructures would all be enhanced by the addition of functional groups, which would supply cross-linking moieties. Moreover, the conductivity and sensitivity of a biosensor based on a chitosan composite/nanocomposite will be much improved.[17] An electrochemical lipocalin-2 (LCN-2) aptasensor was previously described that used a synergistic nanocomposite film made of gold nanourchins (AuNU), oxidized carbon nanohorns (CNH), and chitosan (CS) as an electrode modifier.[10] The significant potential of gold nanoparticles in the development of effective electrochemical biosensing systems is demonstrated by these examples.

Cancer is a serious illness that can and often lead to fatality. People all over the world depend on its early detection through clinical screening using biomarkers that can help detect different cancers early on, enabling prompt medical regimens that lower mortality rates.[18,19] Apolipoprotein A-1 (ApoA1), the primary protein in high-density lipoprotein (HDL), is well known for regulating cholesterol transport. Recent studies suggest that organismal metabolic changes, such as variations in ApoA1 levels and quality, may facilitate the initiation and progression of cancers including ovarian carcinoma, adenocarcinoma, and gastric cancer.[20] Therefore, the establishment of reliable detection techniques for ApoA1 is essential for the early detection and treatment of related conditions. An enzyme-linked immunosorbent assay (ELISA)[21] is usually used to assess the level of ApoA1 molecules in biofluids. However, this method is expensive and requires a long incubation time. Other methods have been similarly employed for ApoA1 detection, such as HPLC[22] and LCMS,[23] but these methods have complex protocols and require relatively long-term skilled labour. Thus, several other approaches have been adopted to overcome such problems and limitations.

Electrochemical biosensors have long been the focus of research due to their robustness, affordability, high sensitivity, and ease of use.[3,24,25] Amongst the diagnostic methods developed to detect low concentrations of proteins are biosensors that incorporate aptamers in their construction, called aptasensors. They have been recognized for their excellent specificity and affinity towards target molecules such as proteins, organic and inorganic molecules, and even whole cells.[17] Aptamers are short synthetic single-stranded DNA or RNA oligonucleotides selected through SELEX (systematic evolution of ligands by exponential enrichment) processes from a random sequence bank.[26] Aptasensors with high affinity and specificity towards a wide variety of target molecules, including proteins, enzymes, antigens, antibiotics, toxins, pharmaceutical drugs, and viruses, have been utilized as powerful molecular recognition tools not only in drug design and delivery but also in analytical bioassay.[27,28]

The detection of ApoA1 has been previously described using electrochemiluminescence (ECL),[29] electrochemical impedance spectroscopy (EIS),[30] and colorimetric immunosensors.[31] However, to the best of our knowledge, ApoA1-specific aptamer-based electrochemical biosensors have not been reported so far. In this study, we take advantage of the simplicity and novelty of the AuNR/AuNW/CS nanocomposite to construct an electrochemical aptasensor for selective and sensitive detection of ApoA1 (Fig. 1). A three-electrode system, consisting of an Ag/AgCl reference electrode, a platinum counter electrode, and a glassy carbon working electrode (GCE), was employed in this work. The nanocomposite was first drop-casted onto the GCE surface. As surface modification impacts sensitivity and selectivity, its incorporation is essential in developing biosensors. Self-assembled monolayers (SAMs) are generally used to

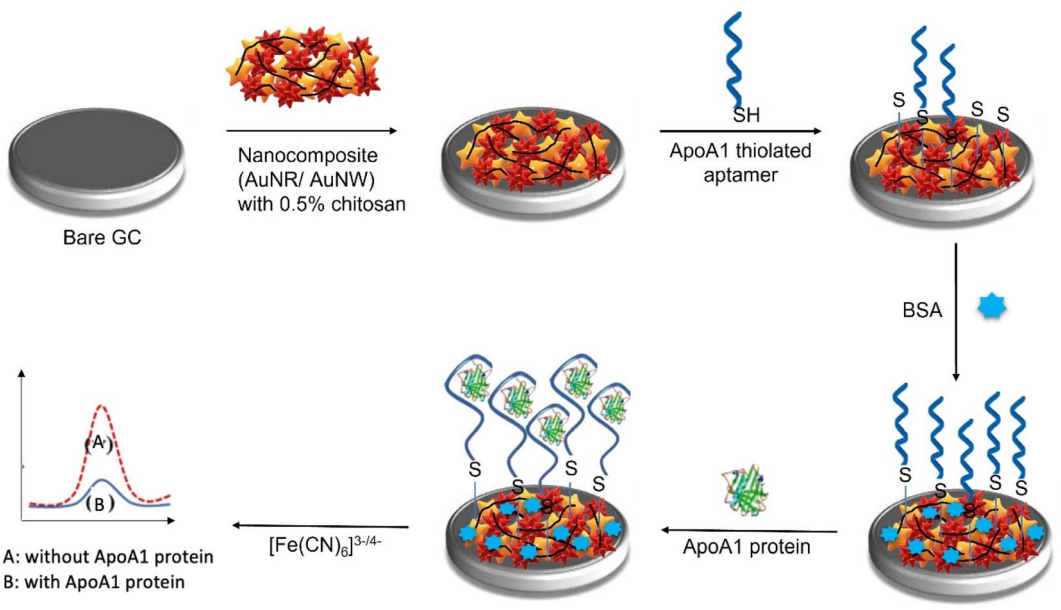

Fig. 1 Schematic representation of the fabrication steps of the ApoA1 aptasensor.

immobilize bioreceptor molecules on gold electrode surfaces, allowing for interaction and passivating the electrode to minimize non-specific interactions. Alkanethiol chemistry is one of the most widely accepted strategies to achieve this objective. On a gold surface, alkanethiols can be readily adsorbed and combined to form a SAM due to the presence of gold-sulfur linkages.[32] For this reason, thiolated ApoA1 aptamers were employed and immobilized on the AuNR/AuNW/CS/GCE surface by establishing SAM between the Au-modified surface and –SH group on the aptamer (Apt/AuNR/AuNW/CS/GCE). The sensing interface was blocked in the presence of ApoA1, and the electron transfer decreased. A label-free electrochemical aptasensor for the detection of ApoA1 was, therefore, created in this study following the alterations of the peak currents in the absence and presence of ApoA1. Our results showed that the reported sensor was sensitive and specific enough to be used to determine the presence of ApoA1 in clinical diagnostics.

Experimental

Reagents and materials

Gold nanorods (AuNRs), gold nanowires (AuNWs), bovine serum albumin (BSA), potassium ferricyanide ($K_3[Fe(CN)_6]$), potassium ferrocyanide ($K_4[Fe(CN)_6]$) were purchased from Sigma Aldrich Co. (Saint Louis, USA). Chitosan (85% deacetylated) was obtained from Alfa Aesar (Ward Hill, M.A). The ApoA1 thiolated aptamer was synthesized by Sangon Biotechnology Co., Ltd (Shanghai, China). The sequence of nucleotides in the aptamer was 5′-thiol-C6-CCTCGGCACGTTCTCAGTAGCGCTCGCTGGTCATCCCACA-3′. The aptamer was reconstituted and then diluted to the desired concentrations using TE buffer. All reagents were of analytical grade, and all solutions were prepared using double distilled water. Thermo Scientific's human ApoA1 ELISA kit was used for this study.

Apparatus and instruments

Ultrasonication was carried out using FB 15046 Fisherbrand® Sonicator. All pH measurements were acquired using Eutech™ pH 700 Meter (Fisher Scientific, USA). All electrochemical measurements, including cyclic voltammetry (CV) and differential pulse voltammetry (DPV), were performed using eDAQ. Glassy carbon electrodes were used as the working electrode, Ag/AgCl electrode as the reference electrode, and a Pt wire as the auxiliary electrode. All electrodes are in a cell containing 20.0 mL 0.01 M PBS (pH 7.4) with 0.1 M KCl solution and 5.0 mM were ($K_3[Fe(CN)_6]/K_4[Fe(CN)_6]$) at room temperature (20 ± 2 °C). All electrodes were purchased from BASi Inc. (IN, USA). All analyses were performed at room temperature, and error bars indicate the standard deviation of at least three replicates ($n = 3$) for all experiments.

Synthesis of AuNR/AuNW/CS

Firstly, 0.5% chitosan solution was added with AuNRs and AuNWs in a ratio of 1 : 1 and sonicated for 1 hour to ensure that the nanomaterials were evenly dispersed. To prepare the nanocomposite, AuNR/CS and AuNW/CS solution were mixed at a 1 : 1 ratio and magnetically stirred for 1 h. The prepared nanocomposite was stored at 4 °C until further use.

Fabrication of the ApoA1 aptasensor

4 μL of AuNR/AuNW/CS nanocomposite was drop-casted onto the working electrodes and dried in an incubator at 40 °C for 15 minutes. After the formation of the thin nanocomposite layer, the electrode was washed carefully with PBS buffer solution to remove any remnants of the unbound nanocomposite. The electrode was then air-dried at room temperature for the following modification step. The AuNR/AuNW/CS/GCE was then drop-casted with 4 μL of ApoA1 thiolated aptamer and incubated for 30 minutes. The electrodes were rewashed with PBS buffer solution to remove any unbound aptamer molecules and dried at room temperature. Later, the modified electrodes were incubated with 0.1% BSA for 30 minutes to block non-reactive ends and prevent non-specific interactions. The electrodes were washed and dried again for the following modification step.

To detect the presence of ApoA1, 4 uL of ApoA1 protein of specific concentration was dropped onto the designed aptasensor and incubated for 30 minutes to allow the formation of the aptamer–protein complex. Later the electrode was rinsed with PBS to remove any unbound ApoA1 molecules. The binding of the aptamer to ApoA1 protein creates a surplus negative charge on the surface of the electrode, and the value of peak current decreases due to the electrostatic repulsion between the negatively charged $[Fe(CN)_6]^{3-/4-}$ and negatively charged density of the ApoA1.

Electrochemical measurements

The layer-by-layer immobilization steps were interpreted by cyclic voltammetry (CV). The parameter for optimizing the analytical performance of the aptasensor was evaluated using differential pulse voltammetry (DPV). CV and DPV were performed in 0.01 M PBS (pH 7.4) containing 5.0 mM $K_3[Fe(CN)_6]/K_4[Fe(CN)_6]$ and 0.1 KCl. 3 μL of varying concentrations of ApoA1 was spiked onto the constructed aptasensor. After 30 minutes of incubation in the desiccator at room temperature, the aptasensor was washed with PBS to remove any unbound protein. DPV was then used for analysis.

Serum sample preparation and analysis

To assess the aptasensor's efficacy to detect ApoA1 in a real human serum sample, blood was obtained from a healthy person and collected in an appropriate serum separator tube (BD Biosciences) and inverted 8–10 times. Further, a tube was let sit for 15–30 minutes at room temperature to allow the blood to clot. After that, the serum was removed and transferred to a new tube and kept at −80 °C for later use. Further, serum was diluted 100× and spiked with different concentrations of ApoA1.

Results and discussion

Characterization of nanomaterials

The morphologies and structure of the prepared nanomaterials AuNR and AuNW were characterized by TEM (Fig. 2A and B). To

demonstrate the effectiveness of the novel nanocomposite, a comparison of the electronic conductivity of the nanomaterials and the nanocomposite was performed using DPV, with 5 mM $Fe(CN)_6^{3-/4-}$ containing 0.1 M KCl as the redox probe. The DPV signal for the bare GCE was observed to be as low as 40 μA (Fig. 3A, curve *a*). The AuNR/CS- and AuNW/CS-coated GCE (Fig. 3A curve b and *c*) was observed to produce better DPV signals when compared to the bare GCE.

Moreover, the peak current of the nanocomplex AuNR/AuNW/CS was almost four times higher (Fig. 3A, curve *d*) than that of the bare GCE, displaying the enhancement of the electronic characteristics of the composite. The relative proportions

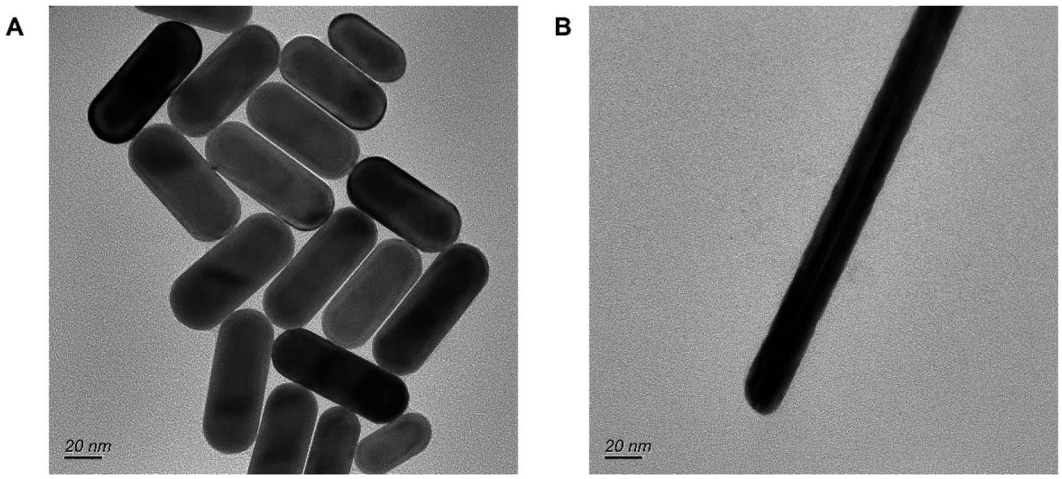

Fig. 2 TEM images of (A) AuNR and (B) AuNW.

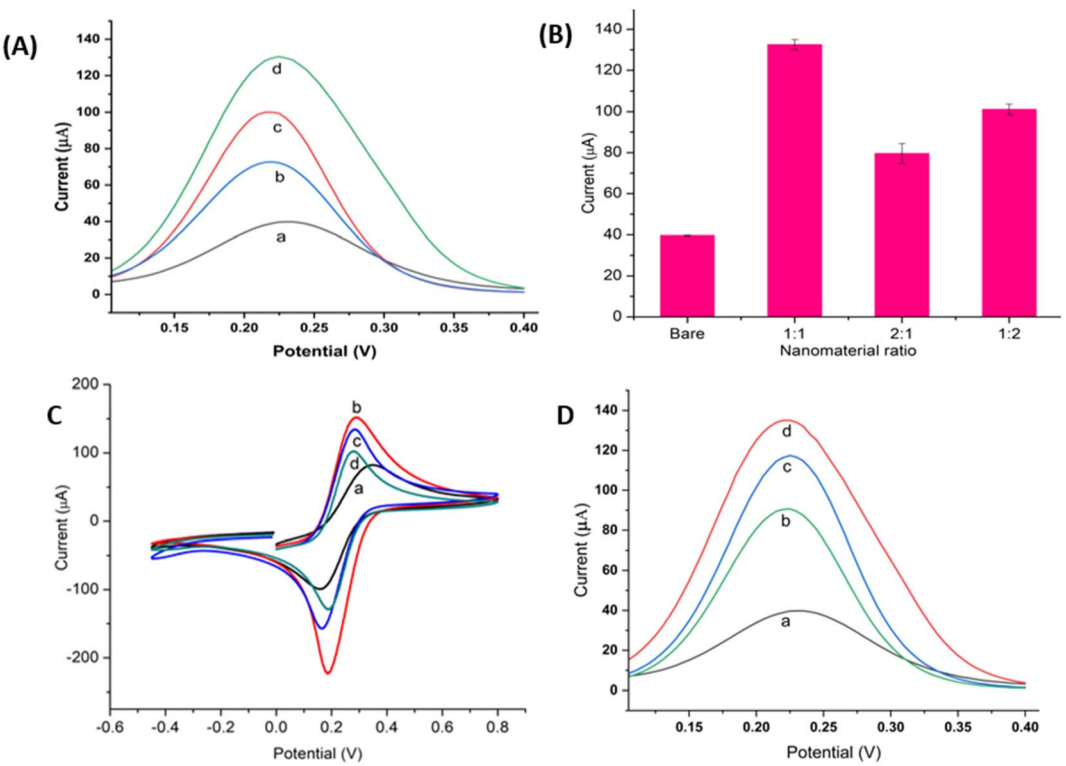

Fig. 3 Characterisation of the nanocomposite: (A) DPV of (a) bare GCE, (b) AuNR/CS (c) AuNW/CS, (d) AuNR/AuNW/CS. (B) DPV peak current of different ratios of AuNR to AuNW in AuNR/AuNW/CS. (C) Layer-by-layer characterization of ApoA1 aptasensor *via* cyclic voltammograms of (a) bare GCE, (b) AuNR/AuNW/CS/GCE, (c) Apt/AuNR/AuNW/CS/GCE, (d) ApoA 1/BSA/Apt/AuNR/AuNW/CS/GCE. (D) Layer-by-layer characterization of ApoA1 aptasensor *via* DPV of (a) bare GCE, (b) AuNR/AuNW/CS/GCE, (c) Apt/AuNR/AuNW/CS/GCE, (d) ApoA 1/BSA/Apt/AuNR/AuNW/CS/GCE. The CV and DPV analysis was investigated in 5.0 mM $[Fe(CN)_6]^{3-/4-}$ containing 0.1 M KCl.

of AuNRs and AuNWs in the nanocomposite might influence the nanocomposite's overall electronic conductivity; hence the AuNR to AuNW ratio in AuNR/AuNW/CS was also optimized by considering the maximum DPV peak current measured. The 1 : 1 ratio of AuNR to AuNW provided the highest peak current, as shown in Fig. 3B, and, therefore, this ratio was used for subsequent experiments.

Electrochemical characterization of the aptasensor

The assembly process of the aptasensor was characterized by CV from −0.7 to 0.8 V in 5.0 mM $[Fe(CN)_6]^{3-/4-}$ and 0.1 M KCl at a scan rate of 100 mV s^{-1}, as shown in Fig. 3C. First, the CV of a bare GCE (curve *a*) was measured, indicating that $[Fe(CN)_6]^{3-/4-}$ has a definite reversible redox activity. Adding AuNR/AuNW/CS nanocomposite to the bare GCE resulted in an increased CV peak current (curve *b*), indicating that the nanocomposite provided an enhanced electroactive surface area and facilitated electron transport. The Randles–Sevcik equation was used to determine the electroactive surface area (*A*) of the bare and nanocomposite-modified GCE.

$$I_p = 2.65 \times 10^5 n^{3/2} A D^{\frac{1}{2}} V^{\frac{1}{2}} C \quad (1)$$

where I_p is the peak current, n is the number of transferring electrons, A is the electroactive area (cm^2), D is the diffusion coefficient (6.7×10^{-6} cm^2 s^{-1}), V is the scan rate (V s^{-1}), and C is the concentration of the electroactive species (mol cm^{-3}).[33] The electroactive surface area was 0.13 cm^2 for the AuNR/AuNW/CS-modified GCE and 0.062 cm^2 for the unmodified GCE. The values supported the fact that the AuNR/AuNW/CS nanocomposite increased overall conductivity due to the increased surface area provided by both AuNR and AuNW. Self-assembly of thiolated aptamer onto the modified electrode surface induced a significant decrease in the CV currents (curve *c*). This reduction indicated that ApoA1-specific aptamer significantly decreased efficient electron transfer area and active sites caused by a repulsive force generated by the aptamer phosphate groups, hence the decrease in the CV signal. When BSA and ApoA1 were introduced, a further reduction in CV signal was detected (curve *d*). The results demonstrated that the binding of aptamer to ApoA1 created a surplus negative charge on the surface of the electrode. The value of the peak current decreased due to the electrostatic repulsion between the negatively-charged ApoA1 protein (the pI of ApoA1 is 5.8 (ref. 34)) and the $[Fe(CN)_6]^{3-/4-}$ redox probe, which resulted in the further signal attrition. Furthermore, the modified electrodes were additionally characterised by DPV from 0.1 to 0.45 V in 5.0 mM $[Fe(CN)_6]^{3-/4-}$ and 0.1 M KCl (Fig. 3D). The addition of the ApoA1 aptamer decreased DPV response (curve *c*) when compared to the nanocomposite modified GCE (curve *b*). Fig. 2D curve *d* showed that the DPV signal was further reduced after being blocked with BSA and having the target protein ApoA1 added onto the sensor surface.

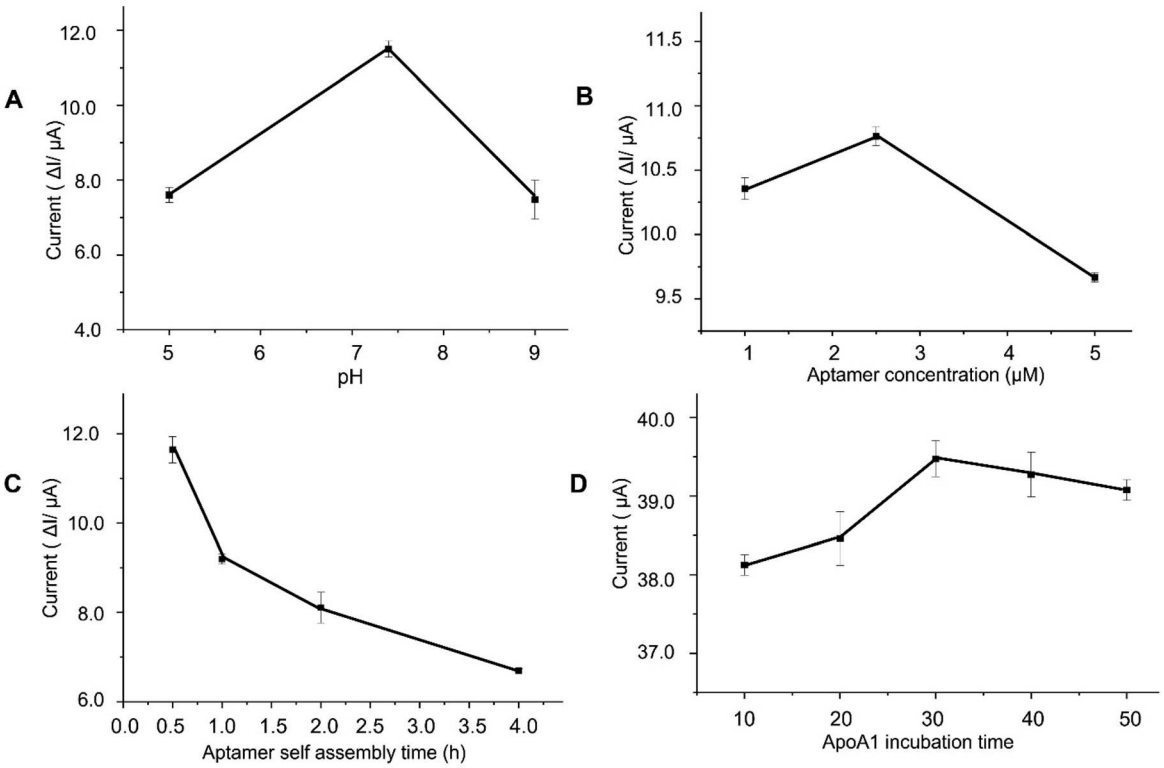

Fig. 4 Determination of optimal experimental conditions for the aptasensor fabrication. Effects of varying (A) pH of the buffer, (B) aptamer concentration, (C) aptamer self-assembly time, and (D) ApoA1 incubation time. All experiments were conducted in 5.0 mM $[Fe(CN)_6]^{3-/4-}$ containing 0.1 M KCl.

Optimisation of the experimental conditions

Optimisation of experimental conditions was essential to ensure the optimal sensitivity and selectivity of the aptasensor. Several variables of aptasensing have been optimised, including pH of the electrolyte, aptamer concentration, aptamer reaction time, and ApoA1 binding time. DPV was utilized for the optimization process in consideration of its higher resolution and current sensitivity. Biological molecules are mostly pH sensitive as it is one of the significant factors that could affect the structure and properties of the aptamer. The pH of the electrolyte for ApoA1 detection was optimized by analysing the current obtained when 100 pg mL^{-1} of ApoA1 was incubated in different pH values of electrolyte (as shown in Fig. 4A). The ΔI value, which is the change in current intensity before and after ApoA1 binding ($\Delta I = I_{apt} - I_{ApoA1}$), was calculated and the optimal DPV response was found to be the highest at pH 7.4. A decrease in performance was observed at pH higher and lower than 7.4, indicating that the acidity and alkalinity of the electrolyte can affect the activity of the aptasensor. Thus, pH 7.4 was selected for subsequent experiments. The aptamer concentration also played a crucial role in the fabrication of the aptasensor. AuNR/AuNW/CS-modified electrode was incubated with different concentrations of ApoA1 aptamer (1, 2.5 and 5 μM) to find the optimal concentration. Fig. 4B demonstrated that the optimum concentration was attained at 2.5 μM since it gave the maximum current value. The ΔI decreased as the aptamer concentration increased to 5 μM. This observation might be due to the excess aptamers on the electrode surface, which prevented the conformational change from occurring when the aptamer binds to the ApoA1 protein, rendering the redox moiety inaccessible to the electrode surface. The ApoA1 aptamer immobilization onto the AuNR/AuNW/CS/GCE was optimized by incubating the aptamer for varying amounts of time (30 min, 1, 2 and 4 h). As shown in Fig. 4C, the ΔI decreased significantly after an incubation time of 1 h. Thus, 30 minutes was chosen as the optimal aptamer immobilization time. The binding time of the ApoA1 protein with the aptamer was also a significant factor in attaining better sensitivity. To determine the optimal binding time, 100 pg mL^{-1} of ApoA1 was incubated with the aptasensor for 10, 20, 30, 40, and 50 minutes. As shown in Fig. 4D, the DPV peak current was observed to intensify with increasing binding time up until 30 minutes, but a steady diminution was observed afterwards. This pattern may be due to the saturated level of the ApoA1-aptamer complex.

Analytical performance of the aptasensor

Different concentrations of ApoA1 were incubated with the aptasensor to analyse the electrochemical response by DPV in 0.01 M PBS (pH 7.4) containing 5.0 mM $K_3[Fe(CN)_6]/K_4[Fe(CN)_6]$

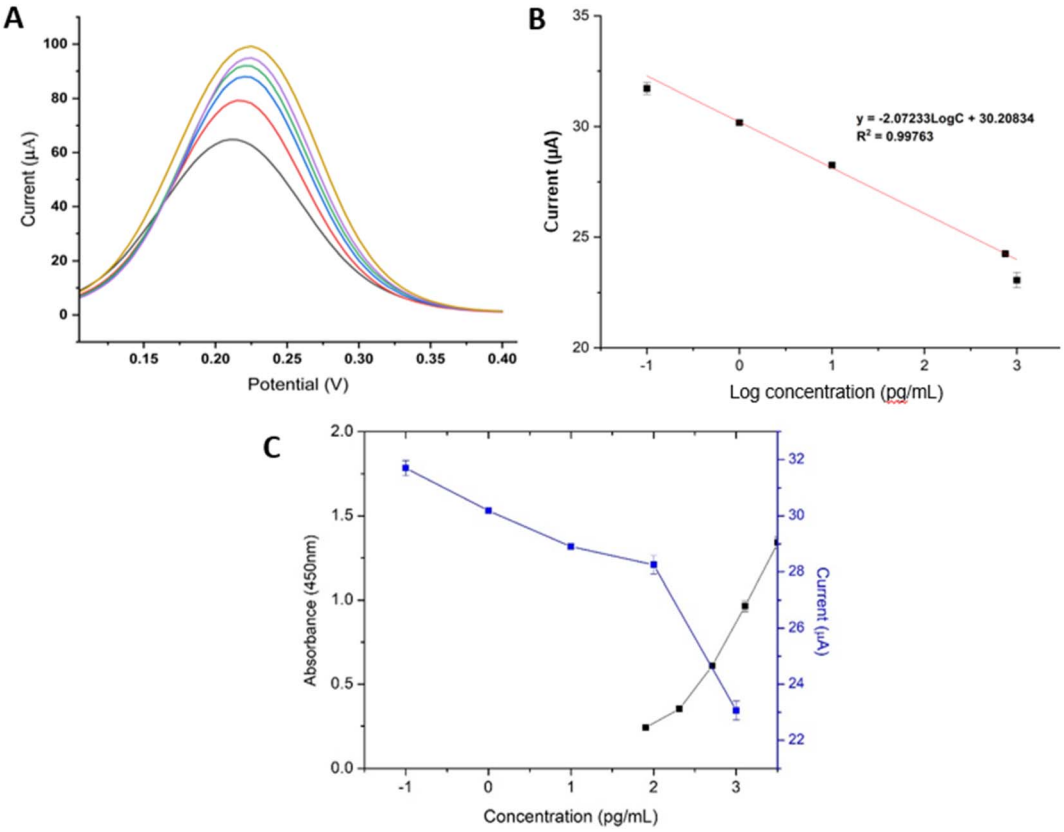

Fig. 5 Analytical performance of the aptasensor. (A) DPV signal of the proposed aptasensor in detecting ApoA1 from concentrations (a) 0.1 pg mL^{-1}, (b) 1 pg mL^{-1}, 10 pg mL^{-1}, (d) 100 pg mL^{-1}, (e) 750 pg mL^{-1} and (f) 1000 pg mL^{-1} (B) the calibration curve of the fabricated aptasensor after incubation with various concentrations of ApoA1 protein. (C) Calibration curve of fabricated EC aptasensor (current) and ELISA (absorbance) for ApoA1 detection.

Table 1 Comparison of the reported analytical capabilities of several ApoA1 detection methods

Methods	Platform	LOD	Linear range	Real sample analysis	Ref.
Impedance immunosensor	Antibody with FuAuNP	50 pg mL^{-1}	0.1–10000 pg mL^{-1}	—	30
ECL immunosensor	AgNCs and carboxyl-functionalized MWCNTs	0.33 pg mL^{-1}	1.0 pg /mL^{-1}–1000 pg mL^{-1}	ApoA1 spiked in human serum samples	29
Fluorescence spectroscopy	Multiplexed MNPs-Abs	7.7 ng mL^{-1}	0.5–3.0 mg mL^{-1}	Blood serum from ovarian cancer patients	35
eELISA	ITO glass strips	1.00 pg mL^{-1}	1.00 fg mL^{-1}–1000 pg mL^{-1}	ApoA1 spiked in urine samples	36
Colorimetric immunosensor	Prussian blue (PB)-incorporated magnetic graphene oxide (PMGO)	0.02 ng mL^{-1}	0.005 ng mL^{-1} – 100 000 pg mL^{-1}	ApoA1 spiked in urine sample	31
The proposed EC aptasensor	AuNR/AuNW	0.04 pg mL^{-1}	0.1 pg /mL^{-1}–1000 pg mL^{-1}	ApoA1 spiked in human serum	This work

and 0.1 KCl. Fig. 5A showed that the DPV current decreased as ApoA1 concentration increased from 0.1 to 1000 pg mL^{-1}. ApoA1 has an isoelectric point of 5.8 and is negatively charged at pH 7.4, which results in a surplus of negative charge on the surface of the electrode and the decrease in the value of peak current due to the electrostatic repulsion between the negatively-charged $[Fe(CN)_6]^{3-/4-}$ and negatively-charged density of ApoA1. DPV results were converted into a calibration curve by plotting the DPV peak current against the logarithmic concentration of ApoA1. Fig. 5B displayed the calibration plot for the ApoA1 aptasensor. A linear relationship between DPV current and logarithmic concentration of ApoA1 was ascertained between concentrations of 0.1 to 1000 pg mL^{-1} (Fig. 5B). The linear regression was determined by the equation $I = -2.06992 \log C + 30.21604$ with a correlation coefficient of $R^2 = 0.99666$. The limit of detection (LOD) of ApoA1 was calculated to be 0.04 pg mL^{-1} using the formula 3 σ/m, where σ was the standard deviation of the blank and m was the slope of the linear curve. The low LOD indicated that the aptasensor has the potential to be used for the detection of trace concentrations of ApoA1. The proposed AuNW/AuNR/CS-based EC aptasensor had a wide linear range and great sensitivity compared to other biosensors for ApoA1 detection (as shown in Table 1). The linear range and detection limits of our ApoA1 aptasensor are also more effective when compared to other EC or ECL sensors that do not utilise aptamers in their construction. Furthermore, the introduction of an aptamer appeared to increase the selectivity of the biosensor. We also used a commercial ApoA1 ELISA immunoassay kit to corroborate the observations of our aptasensor (Fig. 5C). The ELISA had a limit of detection (LOD) of 0.08 ng mL^{-1} (80 pg mL^{-1}), but the aptasensor described here has a LOD of 0.04 pg mL^{-1}, making the ECL aptasensor for ApoA1 approximately 2000 times more sensitive.

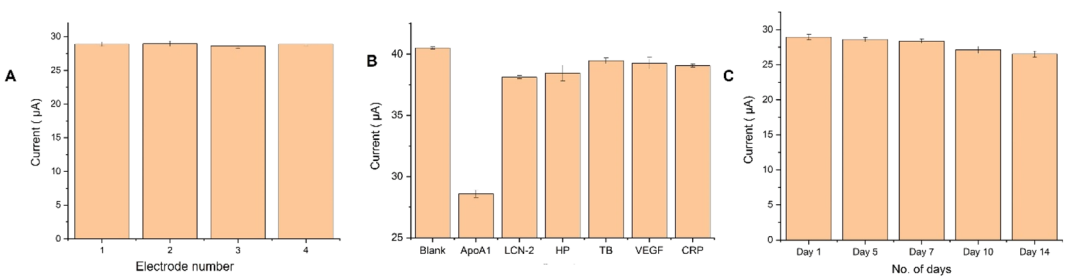

Fig. 6 Reproducibility, selectivity, and stability of the aptasensor. (A) The DPV response of four different aptasensors incubated with 100 pg mL^{-1} of ApoA1. (B) The DPV response of the aptasensor to different serum proteins at 100 pg mL^{-1} concentration. (C) The DPV response of the ApoA1 aptasensor's stability over time (1, 5, 7, 10 and 14 days).

Table 2 Detection of different concentrations of ApoA1 in human serum using the proposed aptasensor

Dilution factor	Spiked concentration (pg mL^{-1})	Determined concentration (pg mL^{-1})	Recovery %	RSD %
100×	0.1	0.100	98.25	0.44
	1	0.681	98.50	2.74
	100	97.67	89.96	1.83
	1000	1000.28	105.14	0.14

Table 3 Comparison of the results obtained by the established electrochemical aptasensor and ELISA with the serum samples

Spiked concentration (pg mL^{-1})	EC aptasensor (pg mL^{-1})	ELISA (pg mL^{-1})	RSD (%)
100	97.67	106	4.7
1000	1000.28	1050	2.6

The reproducibility, selectivity and stability of the aptasensor

The reproducibility of the ApoA1 aptasensor was examined using four different sensors for their detection of 100 pg mL^{-1} ApoA1 (as shown in Fig. 6A). The relative standard deviation (RSD) of the four glassy carbon electrodes was 0.55%, suggesting that the aptasensor exhibited reproducible results. The selectivity of the aptasensor was also analysed to determine the aptasensor's proficiency in identifying ApoA1 from a complex mixture of interfering proteins. The ApoA1 aptasensor was incubated with 100 pg mL^{-1} each of lipocalin-2 (LCN-2), Haptoglobin (HP), Thrombin (TB), Vascular endothelial factor (VEGF), and C-reactive protein (CRP) followed by electrochemical analysis. The obtained DPV peak height was plotted as a bar graph, as shown in Fig. 6B, highlighting the selectivity of the fabricated ApoA1 aptasensor towards ApoA1.The stability of the aptasensor was investigated for its detection of 100 pg mL^{-1} ApoA1 for up to 14 days (Fig. 6C). The aptasensor displayed a modest decrease in signal of only 8.3% even after 14 days, signifying its excellent stability. The excellent nanocomposite used for the aptamer immobilization supported by CS was believed to have greatly increased the stability of the aptasensor.

Real sample analysis

The aptasensor's potential application in real-world samples was tested by detecting ApoA1 in a human serum. ApoA1 was spiked onto a human serum sample using the standard addition method. Various concentrations (0.1, 1, 100, and 1000 pg mL^{-1}) of standard ApoA1 were added to human serum diluted to 100× in 10 mM pH 7.4 PBS buffer. The reliability of the assays was demonstrated in Table 2, with the related standard deviation (RSD) ranging from 89.96% to 105.14%. These results showcased decent reproducibility and consistency. Similarly, it achieved successful recoveries ranging from 0.14% to 2.74%.

Results from the proposed ECL aptasensor were compared to an existing commercial ELISA test. Based on the results shown in Table 3, the suggested ECL approach appears to be in consensus with the ELISA method in terms of detecting the amount of spiked ApoA1 in serum samples (RSD 5%).

Conclusions

In this research work, we have developed a sensitive electrochemical aptasensor of AuNR/AuNW/CS nanocomposite modified GCE for the detection of ApoA1. Chitosan on the modified electrode's surface provided a large surface area for immobilizing an abundance of thiolated ApoA1 aptamers, thereby significantly improving the detection sensitivity. The electrochemical aptasensor displayed high specificity for target ApoA1 in the presence of various interfering substances due to the aptamer's specific recognition and capture capability of aptamer towards ApoA1. With strong selectivity, stability and reproducibility, the proposed aptasensor has a wide linear range (0.1 pg mL^{-1} to 1000 pg mL^{-1}) and a low detection limit of 0.040 pg mL^{-1}. The developed electrochemical aptasensor also presented a good analytical performance in ApoA1 analysis in human serum samples.

Author contributions

Raudhatul Husna: carried out the experiment, prepared the initial draft, and editing; Chitra P Kurup: carried out the experiment, prepared the initial draft, and editing; Mohd Afaque Ansari: carried out the experiment, prepared the initial draft, and editing; Noor Faizah Mohd-Naim: prepared the initial draft, editing and funding acquisition; Minhaz Uddin Ahmed: conceptualization, editing, supervision, project administration, funding acquisition. All authors provided critical feedback and helped shape the research, analysis, and manuscript.

Conflicts of interest

The authors have no conflicts of interest to declare. All co-authors have seen and agree with the contents of the manuscript and there is no financial interest to report. We certify that the submission is original work and is not under review at any other publication.

Acknowledgements

This work was partly supported by the Universiti Brunei Darussalam's grant UBD/RSCH/1.4/FICBF(b)/2018/025, Brunei Research Council Grant-10 and UBD/RSCH/URC/NIG/9.0/2021/001.

References

1 S. A. Lim and M. U. Ahmed, *RSC Adv.*, 2016, **6**, 24995–25014.
2 L. Wu, E. Xiong, X. Zhang, X. Zhang and J. Chen, *Nano Today*, 2014, **9**, 197–211.
3 C. P. Kurup, N. F. Mohd-Naim and M. U. Ahmed, *Crit. Rev. Biotechnol.*, 2022, **42**, 794–812.
4 Y. Liu, X. Liu, M. Li, Q. Liu and T. Xu, *Biosensors*, 2022, **12**(8), 564.
5 S. P. Hong, S. N. A. Zakaria and M. U. Ahmed, *Food Chem. Adv.*, 2022, **1**, 100069.
6 C. P. Kurup, C. Tlili, S. N. A. Zakaria and M. U. Ahmed, *Biointerface Res. Appl. Chem.*, 2021, **11**, 14057–14077.
7 Y. Liu, Q. Xu, Y. Zhang, B. Ren, L. Huang, H. Cai, T. Xu, Q. Liu and X. Zhang, *Talanta*, 2021, **231**, 122360.
8 M. Roushani, B. Zare Dizajdizi, Z. Rahmati and A. Azadbakht, *Nanochem. Res.*, 2019, **4**, 35–42.
9 A. Mohamad, M. Rizwan, N. A. Keasberry, A. S. Nguyen, T. D. Lam and M. U. Ahmed, *Biosens. Bioelectron.*, 2020, **155**, 112108.

10 C. P. Kurup, N. F. Mohd-naim, C. Tlili and M. U. Ahmed, *Anal. Sci.*, 2021, **37**, 825–831.
11 J. Yang, M. Shen, Y. Luo, T. Wu, X. Chen, Y. Wang and J. Xie, *Trends Food Sci. Technol.*, 2021, **110**, 822–832.
12 Y. Song, T. Xu, Q. Zhu and X. Zhang, *Biosens. Bioelectron.*, 2020, **162**, 112253.
13 Y. Lu, X. Zhao, Y. Tian, Q. Guo, C. Li and G. Nie, *Microchem. J.*, 2020, **157**, 104959.
14 S.-H. Shin, G.-Y. Kim, J. Shim, J. Kim, H.-G. Hur, D.-J. Lee, J.-I. Song and S.-H. Moon, *Korean J. Chem. Eng.*, 2012, **29**, 1666–1669.
15 M. Azimzadeh, N. Nasirizadeh, M. Rahaie and H. Naderi-Manesh, *RSC Adv.*, 2017, **7**, 55709–55719.
16 J. Adhikari, N. F. Mohd-Naim and M. U. Ahmed, *IEEE Sens. J.*, 2021, **21**, 4176–4183.
17 C. P. Kurup, N. F. Mohd-Naim and M. U. Ahmed, *Microchim. Acta*, 2022, **189**, 165.
18 V. A. Hristova and D. W. Chan, *Expert Rev. Proteomics*, 2019, **16**, 93–103.
19 J. B. Shah, D. J. McConkey and C. P. N. Dinney, *Clin. Cancer Res.*, 2011, **17**, 2608–2612.
20 K. Georgila, D. Vyrla and E. Drakos, *Cancers*, 2019, **11**(8), 1097.
21 M. Zell, C. Husser, R. F. Staack, G. Jordan, W. F. Richter, S. Schadt and A. Pähler, *Anal. Chem.*, 2016, **88**, 11670–11677.
22 X. Ji, H. Xu, H. Zhang, C. A. Hillery, H.-Q. Gao and K. A. Pritchard Jr, *PLoS One*, 2014, **9**, e91089.
23 Q. Wang, S. Zhang, L. Guo, C. M. Busch, W. Jian, N. Weng, N. W. Snyder, K. Rangiah, C. Mesaros and I. A. Blair, *Bioanalysis*, 2015, **7**, 2895–2911.
24 M. Rizwan, S. Elma, S. A. Lim and M. U. Ahmed, *Biosens. Bioelectron.*, 2018, **107**, 211–217.
25 Y. Liu, Z. Huang, Q. Xu, L. Zhang, Q. Liu and T. Xu, *Microchim. Acta*, 2022, **189**, 91.
26 S. Song, L. Wang, J. Li, C. Fan and J. Zhao, *TrAC, Trends Anal. Chem.*, 2008, **27**, 108–117.
27 C. Padmakumari Kurup, S. Abdullah Lim and M. U. Ahmed, *Bioelectrochemistry*, 2022, **147**, 108170.
28 N. D. Matassan, M. Rizwan, N. F. Mohd-Naim, C. Tlili and M. U. Ahmed, in *2018 IEEE Sensors*, IEEE, 2018, vol. 2018-Octob, pp. 1–4.
29 Y. Zhou, Y. Yu, Y. Chai and R. Yuan, *Talanta*, 2018, **181**, 32–37.
30 S. Zhang, F. Huang, B. Liu, J. Ding, X. Xu and J. Kong, *Talanta*, 2007, **71**, 874–881.
31 C. Peng, M. Y. Hua, N. S. Li, Y. P. Hsu, Y. T. Chen, C. K. Chuang, S. T. Pang and H. W. Yang, *Biosens. Bioelectron.*, 2019, **126**, 581–589.
32 P. Jolly, N. Formisano, J. Tkáč, P. Kasák, C. G. Frost and P. Estrela, *Sens. Actuators, B*, 2015, **209**, 306–312.
33 S. Pei Hong, S. Abdullah Lim, N. Ann Keasberry and M. U. Ahmed, *Bioelectrochemistry*, 2022, **147**, 108172.
34 J. A. Yoo, E. Y. Lee, J. Y. Park, S. T. Lee, S. Ham and K. H. Cho, *Mol. Cells*, 2015, **38**, 573–579.
35 M. K. Pal, M. Rashid and M. Bisht, *Biosens. Bioelectron.*, 2015, **73**, 146–152.
36 S. E. Kim, Y. J. Kim, S. Song, K. N. Lee and W. K. Seong, *Sens. Actuators, B*, 2019, **278**, 103–109.